Plasma Diagnostics for Unraveling Process Chemistry

Joshua M. Stillahn, Kristina J. Trevino, and Ellen R. Fisher

Department of Chemistry, Colorado State University, Fort Collins, Colorado 80523-1872; email: jstill@lamar.colostate.edu, ktrevino@lamar.colostate.edu, erfisher@lamar.colostate.edu

Annu. Rev. Anal. Chem. 2008. 1:261–91

First published online as a Review in Advance on February 26, 2008

The *Annual Review of Analytical Chemistry* is online at anchem.annualreviews.org

This article's doi: 10.1146/annurev.anchem.1.031207.112953

1936-1327/08/0719-0261$20.00

Key Words

deposition, etching, surface modification, gas-surface interactions

Abstract

This review focuses on the use of diagnostic tools to examine plasma processing chemistry, primarily plasma species energetics, dynamics, and molecule-surface reactions. We describe the use of optical diagnostic tools, mass spectrometry, and Langmuir probes in measuring species densities, rotational and kinetic energies, and plasma-surface reactions. Molecule-surface interactions for MX_n species (M = C, Si, N; X = H, F, Cl) are presented and interpreted with respect to the molecule's electronic configuration and dipole moments.

1. INTRODUCTION

T_S: substrate temperature

Plasmas, or partially ionized gases, are complex systems containing a range of reactive species including radicals, metastables, ions, electrons, and photons. Although plasmas can be generated in several ways, they are most commonly created in the laboratory using radio frequency (rf), microwave, or direct current (dc) applied electrical power. Because of the reactive nature of plasma species, a multitude of reactions can occur in the gas phase or at gas-surface interfaces. The result of the interactions of gas-phase plasma species with surfaces (either reactor walls or substrates) generally falls into three categories: (1) etching, or removal of material, often in a selective manner; (2) deposition, wherein a distinctly different chemical material is formed on a substrate; and (3) surface modification, which refers to implantation of chemical functional groups in the outermost surface layer. These processes all rely on a complex set of intertwined chemical reactions that are difficult to understand on a molecular level.

An additional factor contributing to plasma chemistry complexity is the number of system variables used for processes optimization, including equipment variables (reactor size and configuration, materials of construction, method and amount of power applied); gas variables (pressure, flow, and gas ratios); and substrate variables [substrate temperature (T_S), material, and location in reactor]. Often, small changes in a single parameter can result in large changes in the overall process chemistry. In some systems, the balance between etching and deposition is so sensitive to these parameters that controlling the outcome is challenging and miscalculations can result in significant waste. Thus, it is imperative to develop analytical diagnostic tools capable of providing straightforward and reliable process chemistry data.

Understanding fundamental plasma chemistry has been an elusive goal for plasma scientists, primarily because of the systems' complexity. Consequently, relatively little is known about mechanisms for plasma processing. Studies focusing on correlating surface properties with plasma parameters can reveal the nature of the relationships between gas-phase species and processed surface composition. Although these simplistic relationships often offer support for assumptions about deposition and etching mechanisms, they do not directly address gas-surface interface chemistry and thus provide an incomplete picture. A more global representation of molecular-level chemistry is critical, but requires diagnostic tools that (1) allow for the identification and quantification of all plasma species (charged and neutral), preferably temporally and spatially resolved; (2) can be performed in a nonintrusive manner; (3) provide data on the gas phase, surface, and gas-surface interface; and (4) characterize the internal and kinetic energies of plasma species to estimate rate constants and provide energy partitioning information.

Clearly, no one diagnostic tool can fulfill all of these needs. Consequently, many studies that focus on unraveling process chemistry rely on a combination of techniques, affording broader descriptions of plasma processes. As a result of the need for diagnostic tools in both industrial processes and fundamental studies, plasma diagnostics have been the subject of numerous review articles and books (1–4). Here, we focus on a few complex plasma systems that have benefited from the application

of highly sophisticated diagnostic tools to unraveling the underlying molecular-level chemistry.

OES: optical emission spectroscopy

2. DIAGNOSTIC TECHNIQUES

An array of techniques can be applied to the examination of plasma chemistry. Here, we focus primarily on nonintrusive, in situ optical gas-phase diagnostics, although some nonoptical and surface techniques are included. This is by no means an exhaustive list, and detailed descriptions of the instruments can be found elsewhere (1, 5–7).

2.1. Optical Emission Spectroscopy

Optical emission spectroscopy (OES) analyzes light emitted from a given medium in the absence of external excitation via collection, dispersion, and detection of the light (1). In a plasma, gas-phase species are promoted to excited electronic states by collisions with energetic electrons and relaxation is accompanied by emission of a photon. In OES, emitted radiation is spectrally dispersed and detected. In its simplest configuration, OES requires only a means of collecting the light emitted (e.g., an optical fiber), a dispersing element (a grating), and a detector [a photomultiplier tube (PMT) or charge-coupled device (CCD)]. Thus, OES is an inexpensive, real-time monitoring system that can identify emitting plasma species.

OES can be employed quantitatively or qualitatively for plasma species identification and determination of absolute or relative species densities. Identification requires knowledge of the emission lines of a given plasma species (**Table 1**). OES has proven useful in understanding gas-phase kinetics and reaction mechanisms, etching endpoint detection, and performing spatial and temporal measurements of species densities (3, 8, 9). Although quantitative OES is possible, it must be used cautiously because signal intensity is not always directly related to concentration. This is often addressed with actinometry, wherein emission intensities are compared to the relatively constant emission of an actinometer, generally an inert gas (e.g., Ar) or a combination of actinometers added in small quantities. Time-resolved OES (TR-OES) has also been employed (10).

OES is limited to excited-state species that radiatively decay and whose detectable wavelength range is hindered by the collection window, generally precluding vacuum UV (VUV) emitters. Instrument resolution (often only ~0.5–1 nm) and signal-to-noise ratios also limit the utility of OES.

2.2. Optical Absorption Spectroscopy

Optical absorption spectroscopy (OAS) is an alternate probe for excited-state species that measures the light absorbed by a sample at a particular wavelength. OAS is used to probe highly excited molecules because these states are long lived, yet do not decay via emission of a visible photon. Thus, they are not easily probed by OES (1). OAS spectrometers consist of a light source, typically a tungsten-filament or gas-discharge

Table 1 Emission lines observed in optical emission spectroscopy studies of selected plasma species

Species	Wavelength (nm)	Transition	Reference(s)
Ar	696.5	$1s_5-2p_2$	136
	706.7	$1s_5-2p_3$	
	738.4	$1s_4-2p_3$	
	750.4	$1s_2-2p_1$	
	751.5	$1s_4-2p_5$	
	763.5	$1s_5-2p_3$	
	772.4	$1s_5-2p_7$	
	794.8	$1s_3-2p_4$	
	800.6	$1s_4-2p_6$	
	801.5	$1s_5-2p_8$	
	810.4	$1s_4-2p_7$	
	811.5	$1s_5-2p_9$	
	826.5	$1s_2-2p_2$	
	840.8	$1s_2-2p_3$	
	842.5	$1s_4-2p_8$	
	852.1	$1s_2-2p_3$	
C_2	469.8, 471.6, 473.7	$^3\Pi \rightarrow {}^3\Pi$	137
	512.9, 516.5, 558.6	$^3\Pi \rightarrow {}^3\Pi$	
	563.6	$^3\Pi \rightarrow {}^3\Pi$	
C_3	405.1	$A^1\Pi_u \rightarrow X^1\Sigma^+_g$	138
CF_2	251.9	$A^1B_1 \rightarrow X^1A_1$	65, 84
CH	389	$B^2\Sigma \rightarrow X^2\Pi$	116
	430, 431.4	$A^2\Delta \rightarrow X^2\Pi$	117, 139
CN	304.2, 387	$B^2\Sigma^+ \rightarrow X^2\Sigma^+$	116, 140
CO	283, 292.2, 297	$b^3\Sigma \rightarrow a^3\Pi$	137
	302.8, 313.8, 325.3	$b^3\Sigma \rightarrow a^3\Pi$	
	451.1, 483.5, 518.6, 561	$B^1\Sigma^+ \rightarrow A^1\Pi$	
F	685.4	$3p^4D_{7/2} \rightarrow 3s^4P_{5/2}$	141
	703.7, 712.8	$2p^43p \rightarrow 2p^43s$	142
H	434, 486.1, 656.5	$^2P^\circ \rightarrow {}^2D$	137
N	674	$4d^4P \rightarrow 3p^4P^\circ$	116
O	777.2, 844.7	$^3S^\circ \rightarrow {}^3P$	137
NO	247.9, 288.5, 289.3, 303.5, 304.3	$A^2\Sigma^+ \rightarrow {}^2\Pi$	137
	319.8, 320.7, 337.7, 338.6	$A^2\Sigma^+ \rightarrow {}^2\Pi$	
N_2	315.9, 337.1	$C^3\Pi \rightarrow B^3\Pi$	137
OH	281.1, 306.4, 307.8, 308.9	$^2\Sigma \rightarrow {}^2\Pi$	137

lamp, which is directed into a sample chamber, and a detector placed on the opposite side of the sample to analyze transmitted light (11). Thus, OAS is comparable to OES in equipment simplicity.

For gas-phase OAS analyses, the light source can be tuned to a specific optical transition and time-dependent information about a particular species can be obtained. Alternatively, gas-phase absorption can be measured using self absorption, which

has been described in detail elsewhere (12). This allows for quantitative analysis of absorbing species, provided that line shapes and spatial distributions are known.

2.3. Laser-Induced Fluorescence

LIF: laser-induced fluorescence

A common optical plasma diagnostic is laser-induced fluorescence (LIF), which probes ground-state species with sensitivities on the order of 10^8 cm^{-3}. An LIF apparatus generally consists of a tunable laser (e.g., excimer or Nd:YAG-pumped dye laser) and a detector situated orthogonal to the source beam to collect fluorescence. LIF occurs when molecules in the sample volume undergo resonant absorption upon interaction with laser light of the correct wavelength (1, 13). Relaxation via spontaneous emission generates photons that are collected by the detector. The relationship between LIF intensity and the number density of a species depends on intensity of the laser, the transition's quantum efficiency, and the detector's spectral response (7, 13). **Table 2** lists spectral details for specific LIF-probable transitions of plasma species.

Table 2 Spectroscopic properties, dipole moments, relative surface reactivites, and selected laser-induced fluorescence studies of plasma species

Species	Plasma sources	Excited transition	λ(nm)[a]	Radiative lifetime (ns)	Dipole moment (D)	Relative surface reactivity[b]	Reference(s)
C_2	C_xH_y	$A^1\Pi \leftarrow X^1\Sigma^+$	691	1.85×10^4	—	—	143
C_3	C_xH_y	$A^1\Pi \leftarrow X^1\Sigma^+$	410	200	0.44	low/moderate	126, 139
CH	C_xH_y, CH_3OH	$A^2\Delta \leftarrow X^2\Pi$	430	537	0.55	high	117, 139
CHF	CH_xF_{4-x}	$A^1A'' \leftarrow X^1A'$	571	2.45×10^3	1.30	low/moderate	144
CF	C_xF_y	$A^2\Sigma^+ \leftarrow X^2\Pi$	224	26.7	0.64	low/moderate	65
CF_2	C_xF_y	$A^1B_1 \leftarrow X^1A_1$	226	61	0.44	low	65, 84
CCl	CCl_4, CH_4/Cl_2	$A^2\Delta \leftarrow X^2\Pi$	279	105	—	—	145
CN	CH_3CN, CH_4/N_2	$B^2\Sigma^+ \leftarrow X^2\Sigma^+$	387	65	0.50	high	140, 146
NH	NH_3, N_2/H_2	$A^3\Pi \leftarrow X^3\Sigma^-$	336	440	1.39	low/moderate	130
NH_2	NH_3, N_2/H_2	$A^2A_1 \leftarrow X^2B_1$	598	10×10^3	1.82	moderate	130
NO	NO, N_2/O_2	$A^2\Delta \leftarrow X^2\Pi$	226	205	0.16	—	147, 148
OH	H_2O, H_2/O_2	$A^2\Delta \leftarrow X^2\Pi$	308	686	1.80	moderate	28, 149
SiCl	$SiCl_4$, Cl_2[c]	$B^2\Sigma^+ \leftarrow X^2\Pi$	297	10	—	—	150
$SiCl_2$	$SiCl_4$, Cl_2[c]	$A^1B_1 \leftarrow X^1A_1$	320	4.5×10^3	1.46	low	135
SiF	SiF_4, CF_4[c], SF_6[c]	$A^2\Sigma \leftarrow X^2\Pi$	437	230	1.07	moderate	24, 101
SiF_2	SiF_4, CF_4[c], SF_6[c]	$A^1B_1 \leftarrow X^1A_1$	225	6.2	1.23	low	24, 98
SiH	SiH_4, Si_2H_6	$A^2\Delta \leftarrow X^2\Pi$	413	534	0.14	high	20, 107
SiH_2	SiH_4, Si_2H_6	$A^1B_1 \leftarrow X^1A_1$	580	111	0.16	moderate	109
SO	SO_2, SF_6/O_2	$B^3\Sigma \leftarrow X^3\Sigma$	235	16.2	1.55	—	151
SO_2	SO_2, SF_6/O_2	$A^1B_1 \leftarrow X^1A_1$	300	10×10^3	1.63	—	151

[a] Excitation wavelength for listed transition.
[b] Relative reactivity scale: low = < 0.1; low/moderate = ~0.1–0.3; moderate = ~0.3–0.7; high = ~0.7–1.0.
[c] Species of interest is produced during Si processing.

T_g: gas temperature in a plasma

IRIS: imaging of radicals interacting with surfaces, an LIF-based technique

LIF plasma experiments can provide relative and absolute number densities (7, 13–15), gas temperature (T_g), and surface reactivities. LIF techniques that make use of optical evanescent waves, which allow characterization of plasma processes in the near-surface region, can provide relative densities and surface reactivities (16). Other LIF techniques provide data on kinetics (17) and electric fields in plasmas (18). Spatial resolution of LIF signals allows measurement of velocity distributions (19–21), yielding convection and diffusion data (18) and mechanisms for energy partitioning (19, 20). LIF only probes ground-state species, and only those that possess a fluorescing excited state. LIF is not well suited to process control, primarily because of the required laser-system maintenance, and is also hindered by nonradiative relaxation processes.

2.4. Imaging of Radicals Interacting with Surfaces

One special adaptation of LIF as a plasma diagnostic is the imaging of radicals interacting with surfaces (IRIS) technique, which combines molecular beams with spatially resolved LIF to explore radical-surface interactions during plasma processing (22). Gas-phase density and surface reactivity measurements are made as a function of parameters such as applied power (P), substrate material, and T_S. The effects of ion bombardment can be explored using a grounded mesh in the molecular beam path to remove charged species (23), biasing the substrate (19, 24, 25), or employing an alternate, ion-free molecular beam source such as hot-filament CVD (26). IRIS can determine velocities by exploiting the time resolution of the CCD (20, 21, 27), and uses mass spectrometry (MS) to study plasma ions (23, 25).

Figure 1 shows a schematic of the IRIS apparatus (22). In a typical IRIS experiment, feed gases enter a tubular reactor and rf power is applied to produce a plasma. Expansion into a differentially pumped vacuum chamber generates an effusive molecular beam containing virtually all plasma species. A tunable laser intersects the molecular beam and spatially resolved LIF signals are collected by a CCD located perpendicular to the interaction region. For reactivity measurements, a substrate is rotated into the molecular beam path (**Figure 1*a***), and LIF signals are again collected. Differences between spatial distributions with and without the surface (**Figure 1*b***) provide radical-surface interaction data.

Spatially resolved LIF images are interpreted using a quantitative model that reproduces the scattering data in one dimension (22, 28). The model calculates the scattering coefficient (S), which represents the fraction of incident radicals scattered from the surface and is adjusted to best fit the experimental data. For molecules produced at the surface, $S > 1$, whereas for molecules lost at the surface, $S < 1$. Surface reactivity, R, is defined as 1-S and is equivalent to surface loss probability, β, the fraction of gas-phase molecules lost upon interaction with a surface, regardless of loss mechanism.

2.5. Cavity Ringdown Absorption Spectroscopy

Cavity ringdown absorption spectroscopy (CRDS) uses laser pulses to measure absorption of a sample placed directly in the optical cavity of a laser. This is accomplished

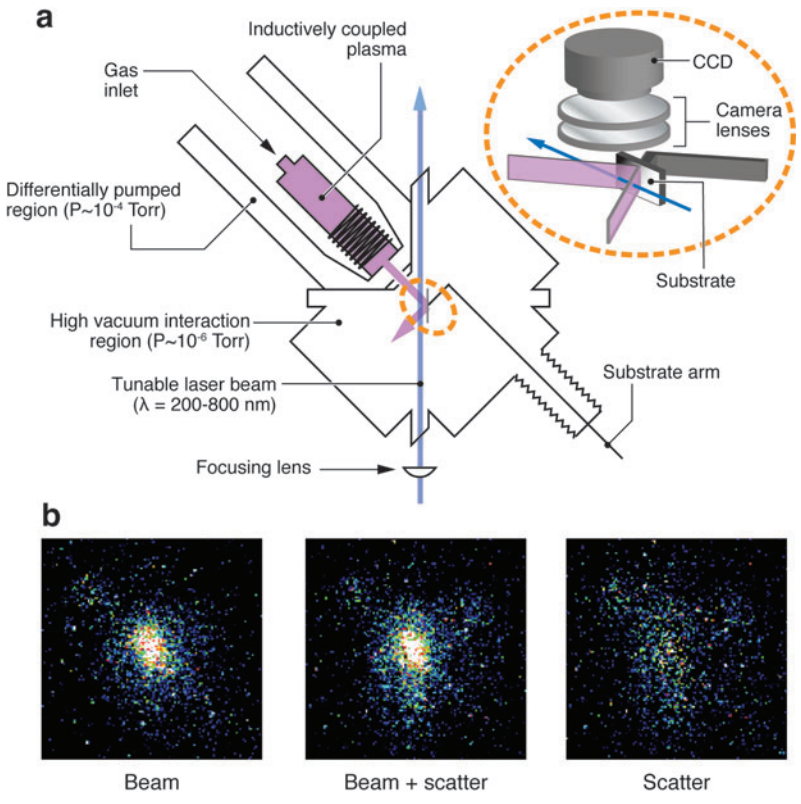

Figure 1

(*a*) Schematic of imaging of radicals interacting with surfaces (IRIS) apparatus. Detail of the interaction region shows the spatial orientation of the optics and detector relative to the molecular and laser beams. Specular scattering of the molecular beam is illustrated. (*b*) Two-dimensional charge-coupled device (CCD) images of CN laser-induced fluorescence (LIF) signals in a CH_3CN plasma molecular beam; CN with a Si substrate rotated into the path of the molecular beam (beam + scatter); and the difference between the other two images, representing only CN molecules scattered from the surface.

by measuring the temporal decay in the intensity of light leaving the laser's output coupler. The time required for the output signal to decay to a fraction, 1/e, of the initial value is the ringdown time, which provides a single-pass transmission coefficient. At nonresonant wavelengths, the ringdown time can be used to correct for effects of mirror reflectivities and cavity dimensions. At resonant wavelengths, sample absorption causes additional signal decay, which can be converted to an absolute absorption (6, 29). Because of its time dependence, CRDS offers increased sensitivity over conventional OAS. CRDS is well suited to plasma systems because the sample is in the laser cavity, providing long effective path lengths and permitting analysis of strongly absorbing species in trace amounts or weakly absorbing species in larger concentrations (30). Although CRDS is less sensitive than "background-free" techniques such

CRDS: cavity ringdown absorption spectroscopy

as LIF and resonant enhanced multiphoton ionization (REMPI), it can be applied when fluorescence and ionization are not practical (29). CRDS can provide absolute densities (31), gas-phase loss rates, and β values (32–34).

N_e: electron density

T_e: electron temperature

TIMS: threshold ionization mass spectrometry

IED: ion energy distribution

2.6. Langmuir Probes

The most widely used electrical plasma probe is the Langmuir probe (11, 35), which measures the plasma current potential (*I-V*) relationship and functions similar to electrodes in electrochemical cells. Probes can be run effectively in potential sweep mode, similar to cyclic voltammetry. From the resulting data, electron and ion distribution functions are derived, providing electron temperature (T_e), electron density (n_e), and plasma potential (V_p). Langmuir probes often have reference electrodes or double probes, wherein a second electrode forms part of the electrical circuit (11, 36). Double probes are preferred as they do not induce as large a perturbation to the plasma, which is critical for probe theory validation. A distinct disadvantage arises from probe contamination from sputtered or deposited material, which can affect the probe's ability to accurately describe V_p (35).

2.7. Fourier Transform Infrared Spectroscopy

Fourier transform infrared spectroscopy (FTIR) is a vibrational spectroscopy applicable across a range of chemistries. FTIR plasma diagnostics focus on both the gas phase and processed surfaces (5, 37). The gas phase can be analyzed as a nonintrusive in situ probe in the exhaust region to monitor plasma effluent (38), which also provides information on plasma-generated species. Determination of parent molecule breakdown in the reactor helps ensure that the desired chemistry is occurring. FTIR analysis of a plasma-processed sample can occur either in situ, by monitoring the gain or loss of a particular species on the substrate, or ex situ, by removing the substrate from the system.

2.8. Mass Spectrometry

Quadrupole mass spectrometers (QMSs) (39) are the most common MS instruments used in plasma diagnostics (40). QMSs provide several analytical advantages, including fast analysis with good sensitivity, compactness, and robustness. In general, a mass spectrometer consists of an ion source, an analyzer, and a detector. A common ionization source is electron impact, which allows adjustment of the electron energy. Threshold ionization mass spectrometry [TIMS, or appearance potential mass spectrometry (APMS)] uses this source for detection of neutral radicals by controlling the ionization energy to selectively ionize plasma radicals over the parent species (39, 41–43).

In addition to providing information about the identity and concentration of plasma species, retarding field analyzers or ion optic elements can be incorporated to characterize ion energy distributions (IEDs). Analysis of IEDs can be used to study the angular distribution of plasma ions (44). This is especially relevant in etching,

where angles of incidence influence etch rates and profiles. Other MS adaptations include cryotrapping-assisted MS, in which successive outgassing of cryotrapped plasma species provides mass spectra in complex deposition plasmas (45), and temperature-programmed desorption, in which a QMS is used to detect desorbing species (46).

2.9. Spectroscopic Ellipsometry and Second Harmonic Generation

Spectroscopic ellipsometry (SE) involves the measurement of changes in the polarization of light when reflected from a surface (1). It is noninvasive and can provide in situ characterization of plasma-deposited films. The experimental ratio of reflection coefficients can be compared to a model of the material structure to determine thickness and dielectric function. Refractive index, microstructure, and density data can also be determined. SE can achieve submonolayer resolution (~0.01 nm), but data quality depends largely on how well the model approximates the experimental system. Although SE is useful in characterizing buried interfaces, analysis becomes increasingly difficult with thicker films. Phase-modulated SE is used as an in situ probe of surface bonds during etching (47, 48).

Second harmonic generation (SHG) is related to SE in that incident light causes variations in the polarization of affected molecules, thereby generating a second electromagnetic field. When this occurs via a linear process, the polarization is linearly proportional to the incoming field, and the generated and incident fields have the same frequency. With more intense light (i.e., from a laser), additional terms must be included; in SHG, these are associated with generation of a field whose frequency is twice that of the incident light (1, 49). SHG signals from an interface are reflected and the polarization components are analyzed, the intensity of which depends on the sample's susceptibility (50). With centrosymmetric media, bulk molecules possess zero susceptibility and do not create a second harmonic response. This symmetry breaks down at a surface (49), and the sensitivity of SHG to interfaces (exposed and buried) is a particular strength. SHG can be applied under many experimental conditions, and does not require sample isolation in vacuum. Thus, it can be performed in situ to obtain time-resolved data on adsorption dynamics, orientation, surface charge, and number density of interfacial species with submonolayer sensitivity (51–53).

3. CHEMISTRY OF SPECIFIC SYSTEMS

Many plasma systems have benefited from the application of a combination of diagnostic tools, which aids the understanding of the synergy between gas-phase chemistry and the resulting process (etching, deposition, or surface modification). Here we review a few selected major systems, with an emphasis on understanding the plasma-surface interface.

3.1. Fluorocarbon Plasmas

Early spectroscopic studies in fluorocarbon (FC) plasmas focused on CF and CF_2, examining spectral characteristics using an FC electrodeless discharge as the CF_x

CCP: capacitively coupled plasma

ICP: inductively coupled plasma

[X]: concentration of species X

source (54, 55); these studies represent the beginning of an understanding of CF_x plasma chemistry and properties. Mathias and Miller examined polytetrafluoroethylene (PTFE) decomposition in microwave discharges, identifying C_xF_y products along with SiF_4, CO_2, CO and COF (56). Proposed mechanisms for plasma-surface interactions included both thermal and radiation-induced reactions. This early work provided a foundation for subsequent studies of FC plasma-surface interactions.

Due to the exceptional etching capabilities of FC plasmas, interest in these plasmas rose dramatically with the development of the microelectronics industry. This is reflected in comprehensive reviews of the recombination chemistry and parameters affecting etched surfaces (57–59). Numerical modeling has also offered insight into FC plasma etching (60, 61). Key findings clearly demonstrate that both ions and neutrals are central to etching and deposition mechanisms. Moreover, it is the synergistic activity of FC species in the gas phase and at the processed substrate surface that allows for the development of FC plasma applications (62).

3.1.1. CF_x density measurements. Identification of gas-phase species and changes in density as a function of plasma parameters can help elucidate plasma chemistry. Thus, many FC plasma studies have measured CF_x and CF_x^+ densities using multiple techniques and by exploring parameter-based trends. Kiss et al. used LIF and OES to measure the relative densities of CF and CF_2 in CF_4/Ar plasmas (63). The two techniques yielded comparable results and showed that LIF results were linearly correlated with actinometric OES results. Booth et al. measured relative CF_x densities and internal temperatures with UV-OAS (64, 65), and employed LIF and CRDS in CF_4 capacitively coupled plasmas (CCPs) to measure absolute CF and CF_2 concentrations (30, 66). CRDS resulted in $[CF] = 6 \times 10^{11}$ cm^{-3} in the reactor center, considerably lower than the result obtained with LIF. The LIF studies demonstrated, however, that [CF] decreased with distance from the electrode. $[CF_2]$ could not be determined with CRDS, but LIF yielded $[CF_2] \sim 6.8 \times 10^{12}$ cm^{-3} near the powered electrode, decreasing with distance from the electrode, similar to CF.

In related studies, [F] in a CF_4 CCP was measured by combined LIF and OES measurements (15). Using $[CF_2]$ measured by LIF and the actinometric OES ratio of I_F/I_{Ar}, where I_F and I_{Ar} are emission intensities of the F and Ar signals, respectively, Cunge et al. (15) determined the absolute [F] with and without a Si substrate. [F] without a Si substrate increased as a function of P to a maximum of $\sim 6.5 \times 10^{14}$ cm^{-3}. With a Si substrate, [F] was substantially lower because etching reactions allow for recombination with etch products. Graves and colleagues measured neutral and ionic number densities in CF_4 inductively coupled plasmas (ICPs) using APMS, QMS, and a Langmuir probe (41, 67). A key result was that $[CF_x]$ varied with wall conditions, suggesting that wall interactions control FC gas–phase chemistry.

FC plasmas are known to selectively etch Si over SiO_2, primarily as a result of different plasma-surface interactions. Miyoshi and colleagues used computerized tomography OES (CT-OES) to measure the spatiotemporal structure of etchants, etch products, and their daughter products during Si and SiO_2 etching in CF_4/Ar mixtures (68). They measured the number densities of excited Ar, Si, SiF, and F and found that [F*] decreased as the Si etching rate increased, whereas [SiF*] increased

during SiO_2 etching. This was attributed to the deposition regime in SiO_2 etching, wherein FC film deposition prevents reactive etchants such as F atoms and CF_x^+ ions from reaching the underlying SiO_2 layer. Studies such as these provide insight into selective etching mechanisms in FC plasmas.

$\Theta_R(MX_n)$: rotational temperature of a given species

3.1.2. Fluorocarbon plasma dynamics. Understanding the dynamic processes that influence plasma species behavior is critical to refining overall etch or deposition processes in FC plasmas. The kinetic behavior of plasmas relies heavily on the energies of its constituents; thus, measurement of T_e and T_g provides one method for examining energy distribution in a plasma. Donnelly and colleagues applied trace rare gases OES (TRG-OES) to measure T_e and T_g in C_2F_6/C_4F_8 plasmas (69). The feed gas also included a carrier gas and multiple inert probe gases (He, Ne, Ar, Kr, and Xe). The emission behavior of probe gases is predictable from excitation cross sections and relaxation processes. Each gas is sensitive to a different part of the electron energy distribution function; collectively, the gases' emission intensities provide a description of T_e. Emission spectra with N_2 as the probe were used to characterize T_g from analysis of N_2 rotational spectra. Both T_e and T_g were strongly dependent on carrier gas, suggesting that careful selection of carrier gas could provide another degree of control over the energies of plasma species.

Measurements of internal and translational energies of plasma species also provide estimates of T_g. Nagai and Hori measured the rotational temperature (Θ_R) of CF in CF_4 and CF_4/Ar plasmas using OES and infrared laser absorption spectroscopy (IRLAS) (70). Θ_R increased from 300 to 380 K as P increased from 375 to 1500 W, and was accompanied by a ~threefold increase in [CF]. With CF_4/Ar, Θ_R and [CF] were substantially lower, with Θ_R only increasing by ~20 K over the same P range. This likely resulted from increased elastic collisions leading to CF rotational cooling, and demonstrates that rotational heating is not appreciable in these systems. Similar values were obtained using planar LIF to create two-dimensional maps of Θ_R(CF) in CF_4 CCPs (71). Θ_R displayed strong gradients, increasing with distance from electrodes. These results have implications for density and kinetics studies that examine only a single rotational state.

Both negative and positive ions significantly influence FC plasma etching processes. Negative ion decay occurs only through ion-ion recombination in the plasma bulk. Hebner and colleagues used photodetachment spectroscopy to measure the F^- absolute density in CF_4, C_2F_6, and CHF_3 plasma afterglows (72). The $[F^-]$ time-dependence yielded ion-ion recombination rates of 0.88×10^{-6}, 1.5×10^{-6}, and 3.9×10^{-6} cm^3/s for CF_4, C_2F_6 and CHF_3, respectively. Positive ions can strongly influence the net rate of ion-ion recombination. The dominant positive ion is CF_3^+ for CF_4 and C_2F_6 plasmas, but CF_2^+ dominates CHF_3 plasmas, suggesting that CF_2^+ enhances ion-ion recombination rates in FC plasmas.

Hancock et al. measured F-atom emission at different delay times after the power-off in FC plasmas using TR-OES (10). Decay was attributed to gas-phase recombination processes and losses at the reactor walls. Addition of a Si substrate increased etching reactions, thereby dramatically increasing the decay, whereas addition of O_2 significantly increased [F]. UV-OAS results from studies by Sasaki et al. (73)

$\beta(MX_n)$: surface loss probability; the fraction of molecules lost from the gas phase upon interaction with a substrate

contained rapid decay in [F] in the initial afterglow of their CF_4 plasma, followed by an exponential decay in [F] at longer times. This was attributed to the initial reaction of CF_x on reactor walls and simple diffusion to, and loss at, wall surfaces in the afterglow. These mechanisms are supported by the QMS, Langmuir probe, and OES studies by Sugai et al. who found that heated reactor walls (100–200°C) resulted in large increases in [CF_x] (74). Using in situ FTIR, OES, and ex situ attenuated total reflectance (ATR)–FTIR, Goeckner and colleagues (75) found that CF_x was lost on low-temperature walls in CF_4 plasmas, but preferentially desorbed at high temperatures. They also concluded that both film deposition and etch rate were determined by two major competing processes, direct ion incorporation and ion-assisted surface desorption.

3.1.3. Surface interactions. In FC plasmas, etching and deposition are competitive processes and often occur simultaneously (57). Species density studies as a function of plasma parameters reveal that film formation and etching are controlled by the interactions of plasma species with a substrate. The balance between highly energetic ions and neutral radicals bombarding the substrate being processed dictate the dominant process.

3.1.3.1. Radical-surface interactions. Radical-surface interactions are key steps leading to FC film deposition and to etching of Si substrates. In general, it is assumed that when radicals impinge on a surface, they react with unit probability, essentially the first step in all three radical-surface processes depicted in **Figure 2*a***. Indeed, this assumption is regularly made in computer simulations where no experimental data are available. Surface loss, however, can occur via several different processes, including dissociative adsorption (**Figure 2*a***, *process 2*), or surface atom abstraction (**Figure 2*a***, *process 3*). In both cases, the newly formed species can subsequently desorb (as shown), but whether desorption occurs or not, these processes contribute to β. Although the first step of process 1 depicts simple adsorption, which contributes to β, subsequent desorption would result in higher *S*. CF_x (x = 1–3) species are proposed critical components in FC polymerization (76–78). Radicals contribute to polymer growth by reacting with "activated" sites on the polymeric surface or by forming addition compounds through gas-phase reactions. Despite these predicted behaviors, growth mechanisms remain unclear, and β values measured *during* plasma-surface interactions are critical to full understanding (79).

$\beta(CF_x)$ appears to vary dramatically with plasma gas chemistry, surface conditions, and wall history. For example, Booth and colleagues used LIF to measure $\beta(CF) = 0.06–0.24$, depending on [F(g)] (66, 80). APMS measurements of $\beta(F)$ and $\beta(CF_x)$ on the walls of an ICP reactor were strongly dependent on wall conditions (81). Hikosaka et al. found that $\beta(CF_2)$ and $\beta(CF_3)$ measured by TIMS were nearly identical in CF_4 plasmas (~0.13), but that β decreased by $\sim 10^2$ for both species when H_2 was added (82). In general, CF_x (x = 1–3) species have low β, and all appear to be strongly coupled to the conditions under which measurements are made.

IRIS studies demonstrated that CF_2 is generated at surfaces (i.e., $S > 1$; $\beta < 0$) under etching conditions (e.g., 100% C_2F_6 plasmas); however, $\beta \sim 0.2$ when a-C:F,H films are produced from 50/50 C_2F_6/H_2 plasmas (76). IRIS studies of CF_2

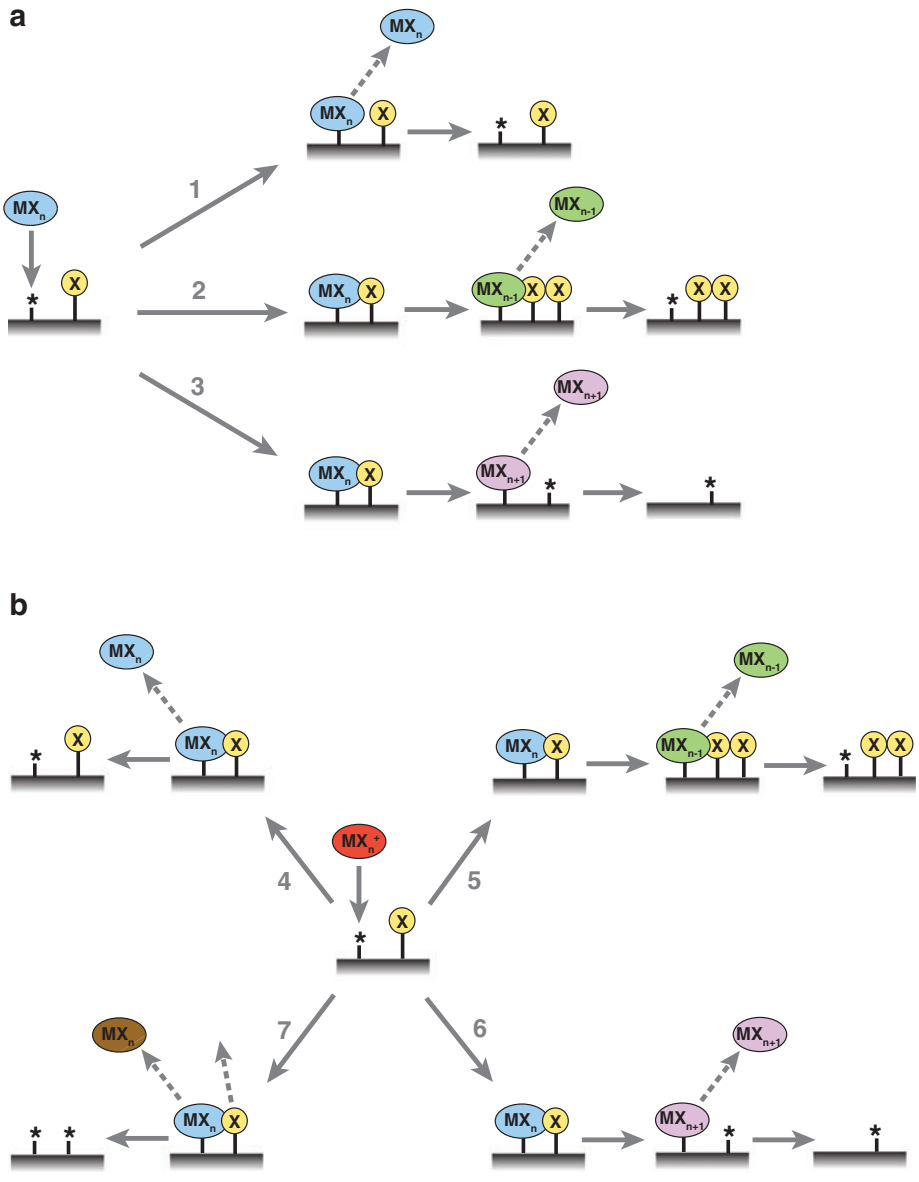

Figure 2

Generalized schematic representation of (*a*) neutral plasma species and (*b*) ionic plasma species interacting with a substrate, where M = C, Si, or N; X = H, F, or Cl; and asterisk represents an active surface site. Process 1 represents simple adsorption-desorption from a surface, usually with thermal equilibration. Processes 2 and 3 represent dissociative adsorption with subsequent desorption of MX_{n-1} and adsorption followed by surface recombination and desorption of MX_{n+1}, respectively. Processes 4–6 are similar to processes 1–3, but include surface neutralization of the incident ion. Process 7 represents ion-induced sputtering, wherein multiple volatile reaction products can be formed.

$\langle E_i \rangle$: mean ion energy

$S(MX_n)$: surface scattering coefficient; represents the fraction of incident molecules scattered from a substrate

using hexafluoropropylene oxide (HFPO), CHF_3, C_3F_8, and C_4F_8 plasmas (76, 77, 83, 84) have yielded three key observations: (1) $S(CF_2)$ is nearly always greater than unity, indicating surface generation of CF_2 during FC processing; (2) $S(CF_2)$ increases with P; and (3) $S(CF_2)$ decreases under ion-free conditions. Time-resolved UV-OAS data for C_2F_4 and HFPO CCPs also found significant CF_2 surface production (85). Booth and colleagues determined that both CF and CF_2 are produced at surfaces in CF_4 plasmas (15, 66, 80). Their proposed mechanism relies on energetic ion-surface interactions producing CF_x, either through CF_x^+ neutralization, (**Figure 2*b***, *process 4*) or via film sputtering (**Figure 2*b***, *process* 7). With no ion bombardment, many surfaces act as CF_x sinks. These observations indicate CF_2 surface production is strongly correlated to plasma ions. Indeed, Martin et al. found a positive linear correlation between mean ion energy ($\langle E_i \rangle$) in C_3F_8 and C_4F_8 plasmas and $S(CF_2)$ (23). An additional correlation was observed between $S(CF_2)$ and FC film crosslinking for several FC systems (86). Conditions leading to highly crosslinked films result in higher $S(CF_2)$. Overall, when the surface is not bombarded by energetic species (e.g., ions), CF_2 is contributing to film formation, resulting in a more ordered (high CF_2 content) material (26).

3.1.3.2. Ion-surface interactions. As the above evidence demonstrates, ions clearly play a significant role in both FC plasma etching and deposition; possible ion-induced mechanisms are shown in **Figure 2*b***. To clarify this role, the behavior of ions or groups of ions in an isolated environment has been investigated. Sawin and colleagues used individual beams of CF_2, F atoms (created from HFPO pyrolysis and F_2/Xe discharges, respectively), and Ar^+ to simulate the CF plasma etching environment (87, 88). Butterbaugh et al. found that the etch yield saturates at lower radical flux values when the surface is bombarded with higher-energy ions (87). This was attributed to ion-induced surface roughness producing more active sites and higher β.

Hanley et al. examined ion-surface interactions using mass-selected beams of $C_3F_5^+$ or $C_2F_4^+$ ions (89, 90). Ions were accelerated or decelerated into a surface to examine the effects of incident ion energy on the properties of the resulting films, as measured by X-ray photoelectron spectroscopy. Ion identity and energy strongly affected film thickness and morphology, but not film composition. Goyette et al. used an electrostatic energy analyzer to examine IEDs and ion flux of CF^+ and CF_3^+ in C_2F_6 and C_4F_8 plasmas (91). At higher pressures, ion flux increased, as did rf modulations, and IEDs were highly dependent on ion mass. Martin et al. measured IEDs and determined $<E_i>$ in C_3F_8 and c-C_4F_8 plasmas (23). IEDs did not exhibit a strong dependence on ion mass, but clearly showed evidence of sheath effects, as $<E_i>$ was relatively high. Increases in $<E_i>$ were linearly correlated to $S(CF_2)$.

3.2. SiF_x Species

In plasma etching (e.g., FC plasmas), SiF_x species can be volatile etch byproducts, but they can also act as deposition precursors. Thus, there are many similarities between CF_x and SiF_x plasma species, and optical diagnostics can elucidate both parent FC gas dissociation and etch-product behavior (92, 93). Early SiF_x studies originated

with spectroscopic and thermodynamic measurements using plasma sources (94–96). Subsequent studies focused on parameter dependence in processing systems. Hebner measured [CF_x] and [SiF_x] (x = 1, 2) with LIF, and found that [CF_x] decreased with P and increased with pressure (97). In contrast, [SiF_x] increased with P and pressure in C_2F_6 and CHF_3 plasmas, but was independent of pressure for C_4F_8 plasmas. These results suggest that C_2F_6 and CHF_3 are more efficient Si etchants than C_4F_8. CT-OES studies of Si and SiF demonstrated that production of SiF occurs via gas-phase dissociation of etch products. Other LIF studies distinguished between SiF production in the presence of ion bombardment and by chemical etching of F atoms (98).

3.2.1. SiF_x dynamics. Giapis and colleagues obtained gas-phase and surface kinetics for SiF_x species using MS (99, 100). For SiF_x^+ (x = 1–3), the time-of-flight (TOF) distributions contained two components, which were attributed to thermally equilibrated species and hyperthermal products of surface reactions. Increases in T_S caused a sharp drop in the SiF_3^+ high-energy component, suggesting that the mechanism favors direct surface reactions for SiF_3 formation.

IRIS studies measured Θ_R for SiF and SiF_2 by comparing surface reactivities for different rotational transitions over a range of T_S (101). This method accounts for changes in rotational state populations for molecules that thermally equilibrate at a substrate, which can result in measured β values being larger or smaller than the true value. When $T_S = \Theta_R$ for the beam species, the state population distribution will not change upon equilibration at the surface, and β for all transitions should coincide. This analysis yielded $\Theta_R(SiF) = 450 \pm 50$ K and $\Theta_R(SiF_2) = 752 \pm 100$ K for a 170-W SiF_4 plasma. Assuming that the SiF_4 parent gas measured ~300 K, these values suggest that thermal equilibration did not take place during surface interactions of SiF_x (27).

3.2.2. Surface interactions. Cunge et al. measured [SiF_2] above Si and SiO_2 substrates in a CF_4 CCP using spatially resolved LIF (98). SiF_2 surface generation should produce a linear decrease in [SiF_2] away from the substrate, and gas-phase loss or production processes would predictably alter concentration profiles. For Si and SiO_2, no net production of SiF_2 was observed, suggesting that SiF_2 is produced primarily at the substrate as an etch product. Data from the plasma afterglow characterized concentration profiles under ion-free conditions. At 50 mTorr, profiles collected 2 ms after rf power interruption revealed that SiF_2 continued to be produced at the Si substrate, but was lost on SiO_2. This suggests that SiF_2 production from Si results from chemical processes, but production from SiO_2 relies on other species such as ions. At 50 mTorr, $\beta(SiF_2)$ estimates were 0.8–1.0 and 0.5–0.6 for Si and SiO_2, respectively. At 200 mTorr, β decreased to 0.04 and 0.11 on Si and SiO_2 substrates, respectively.

Williams & Fisher used LIF, QMS, OES, and ex situ FTIR to study SiF_x surface interactions during etching and deposition from SiF_4 plasmas (24, 101). They found that T_S significantly affected mechanisms for SiF_x surface desorption and surface adlayer composition (101). Higher T_S resulted in increased SiF and SiF_2 scatter, presumably from increases in process 1 (**Figure 2*a***), although processes 2 and 3 could also contribute. Thus, elevated T_S increases etching efficiency by enhancing

$\Theta_T(MX_n)$: translational or kinetic temperature of a given species

etch product formation. Another IRIS study examined ion influence on SiF_2 surface interactions (24) using a grounded mesh and application of ± 200 V substrate bias. Changes in $S(SiF_2)$ demonstrated that SiF_2 surface generation is ion induced (**Figure 2*b***) and that the amount of SiF_2 generated depends more on energy transfer to the surface than on the availability of chemical etching species (e.g., F).

Interestingly, ion-induced processes did not strongly influence SiF surface interactions, with $\beta(SiF) \leq \sim 0.8$, depending on the overall plasma chemistry (25, 101). The combination of SiF_2 and SiF IRIS data suggests that SiF is primarily a deposition precursor, whereas SiF_2 is a major etch product. IRIS studies at elevated T_S found that $\beta(SiF_2)$ decreased with T_S (300–575 K), a change attributed to changing surface adlayer composition (101). For SiF and SiF_2, β increased for $T_S >$ 575 K as a result of exceeding the desorption energy threshold. TOF-MS studies of SiF_x etch products suggest that ion-surface interactions have two components (99, 100), one that corresponds to ion equilibration at the surface (**Figure 2*b***, *process 4*), and another that produces energetic surface reaction products. Thus, by controlling processes that generate high-energy species, anisotropy and undercutting issues in reactive ion etching processes may be resolved.

In another study, SiF and SiF_2 velocities derived from changes in time-delayed LIF images were converted to translational temperatures (Θ_T) (27). As P increased from 80 to 200 W, $\Theta_T(SiF)$ and $\Theta_T(SiF_2)$ increased from ~570 K to 870 K and from 430 K to 560 K, respectively. Differences in Θ_T for the two species were attributed to differences in mass, as lighter species gain more translational energy. Increases with P were ascribed to increases in ion density, n_e, and collision frequency that accompany higher P. These studies established that plasmas are not always thermally equilibrated and that T_g estimates from a single species in any plasma should be applied cautiously.

3.3. SiH_x Systems

Amorphous, hydrogenated silicon (a-Si:H) has been extensively studied because of its widespread use as an inexpensive solar cell material (102). Although a-Si:H can be produced by a variety of methods, it is most often grown using SiH_4 or Si_2H_6 plasmas, which have afforded a plethora of fundamental experimental and theoretical studies of gas-phase kinetics, thermodynamics, film characterization, and SiH_x measurements (103–105).

3.3.1. SiH_x energetics. Stamou et al. measured $\Theta_R(SiH)$ in SiH_4 CCPs using spatially resolved OES (106). Θ_R linearly decreased with increasing distance from the rf electrode from ~2500 K to ~1975 K at 5–16 mm. This was attributed to the sensitivity of Θ_R to high-energy electrons, which are more abundant near the electrode. $\Theta_R(SiH)$ peaked 5 mm from the electrode, whereas $[SiH^*]$ was highest 7 mm from the electrode. This suggests that the region closer to the electrode has more high-energy electrons, even though n_e is lower. Further from the electrode, emission intensity decreased because less SiH_4 dissociation occurs.

IRIS studies determined $\Theta_R(SiH)$ and $\Theta_T(SiH)$ as a function of P and Ar dilution (20, 107). $\Theta_T(SiH) > \Theta_R(SiH)$ at all P and both are relatively constant at $P >$ 20 W

(20). $\Theta_R \sim 500$–600 K in all feed gas mixtures, indicating that thermal equilibration of rotational energy was established (107). Differences in Θ_R(SiH) in different studies likely result from differences in plasma configurations. $\Theta_T(SiH) > \Theta_R(SiH)$ under most Ar dilution conditions, averaging ~1000 K, although in the Si_2H_6/Ar system, $\Theta_T(SiH) \sim \Theta_R(SiH)$ at the highest Ar dilutions. This suggested equilibration occurs more slowly for translational energy than for rotational energy, and translational energy is equilibrated at different rates in the two silane systems.

3.3.2. Surface interactions. van de Sanden and colleagues utilized an aperture-well assembly to measure a global β value for SiH_x in Ar/H_2/SiH_4 plasmas (108). This apparatus is formed by two substrates 0.5 mm apart, with a 0.1-mm slit in the upper substrate. Radicals adsorb at the lower substrate or are reflected to the underside of the top substrate. Deposition profiles as a function of H_2 flow were related to a global β of < 0.5, which decreased with H_2 flow. This may indicate a role for SiH_3, which decreases in density with the addition of H_2.

Individual contributions of Si and SiH to film growth were derived from the comparison of CRDS-measured densities with simulated data (31). Experimental and simulation results suggest that at low SiH_4 flows, SiH radicals are lost to charge transfer with Ar^+. SiH production reached a maximum at high SiH_4 flows, where the molecules are predominantly lost in reactions with SiH_4. β(Si) and β(SiH) were used to correlate gas-phase densities to film growth contributions, which revealed that Si and SiH contributions are only weakly dependent on H_2 flow. Time-resolved CRDS measurements also provided estimates for β (33). Si and SiH_3 loss rates yielded β(Si) ~1 and $\beta(SiH_3) \sim 0.3$ in Ar/H_2/SiH_4 plasmas. The latter value was independent of T_S (104), indicating that surface reactions occur during film growth. IRIS results confirm that $\beta(SiH) \sim 1$, regardless of plasma parameters, feed gas, and T_S (20).

Few studies have focused on SiH_2 surface interactions, primarily because of its high reactivity and therefore low density in silane plasmas. Decay in [SiH_2] measured by LIF in the afterglow of Ar/H_2/SiH_4 plasmas found that $\beta(SiH_2) = 0.6 \pm 0.15$ (109). TIMS measurements of SiH_3 and Si_2H_5 decay rates in the same apparatus were related to β values using assumptions about surface processes, yielding $\beta(SiH_3) = 0.28 \pm 0.03$ and $\beta(Si_2H_5) \sim 0.1$–0.3 (110). In general, molecular dynamics simulations compare favorably with experimental values for $\beta(SiH_x)$ (111–113).

3.4. CH_x Plasma Chemistry

Although methane plasmas are widely used to deposit a-C:H films, most studies have focused on film properties, providing scant data on gas-phase processes (114). The predominant species in methane plasmas are CH_3 and H atoms (115). MS studies show, however, that larger C_xH_y ($x > 1$) molecules are formed in hydrocarbon plasmas (114, 116).

3.4.1. Energetics. Energy distribution characterization in CH_4 plasmas focused on measuring Θ_R(CH) and on measuring Θ_T(CH) in CH_4/Ar plasmas with LIF (117). Θ_R was ~1450 K, independent of P and [Ar]. However, Θ_T(CH) was significantly

higher than Θ_R, decreasing from 9000 K to 2500 K as P increased from 20 to 100 W, plateauing at $P > 100$ W. A similar trend was observed in [CH], and collectively, these results were attributed to plasma coupling modes. [Ar] did not significantly affect Θ_T, but lower Θ_T occurred at higher pressures, mimicking T_e. Thus, CH is rotationally very hot and is not thermally equilibrated, with the disparity becoming more pronounced at lower P and lower pressures. In situ FTIR spectra were used to derive $\Theta_R(C_2H_2)$ in an expanding thermal arc plasma (118). Although these measurements were unreliable where C_2H_2 consumption was high (low absorbances), simulated spectra reproduced the experimental data, yielding $\Theta_R \sim 300$–450 K, with no dependence on gas flow.

3.4.2. Surface interactions. van de Sanden and colleagues used TIMS, Rutherford backscattering, and ellipsometry to study film properties and C_xH_y species as a function of the C_2H_2/Ar flux ratio, F (119, 120). Radical densities' ($\sim 10^{16}$–10^{17} m^{-3}) dependence on F was modeled and ultimately related to β. For $F < 1$, C and C_2 dominate the gas phase and are strong contributors to film growth, whereas for $F > 1$, radicals with an odd number of carbons contribute the most. Ellipsometric refractive indices were used to correlate C_3 radical density to a-C:H film quality.

CH and H radical beams in conjunction with isotope labeling and in situ ellipsometry studies reveal a-C:H deposition mechanisms (115, 121, 122). Under CH_3 radical flux, the surface coverage of methyl groups reaches a steady state. With H-beam flux, generation of active sites occurs via surface hydrogen abstraction. This leads to film erosion as neighboring active sites relax to form C-C bonds. Alternatively, active sites promote chemisorption of CH_3 and subsequent film growth. Ion-induced processes were studied by exposing surfaces to CH_3 and He^+ beams, wherein film growth was promoted via ion-induced creation of reactive sites. In plasmas, the presence of both ions and H influences film formation. The importance of H flux is supported by $\beta(CH_3)$, which increases from 10^{-4} to 10^{-2} with H atom flux, as well as by isotope-labeling studies. Controlled exposure to D-labeled beams results in surface composition changes that suggest that active sites can be created several monolayers deep. Deeper active sites form C-C bonds, whereas shallow sites promote CH_3 chemisorption.

Time-resolved TIMS in CH_4 plasma afterglows provide $\beta(CH_3)$ values from $[CH_3]$ decay (110). Results show that $\beta(CH_3)$ decreases from $\sim 10^{-2}$ in the plasma to $\sim 10^{-3}$ ms after discharge termination, indicating that active site quenching occurs rapidly. The spatially resolved TIMS results published by Sugai et al. yielded $\beta(CH_3) = 0.001$ and $\beta(CH_2) = 0.028$ (123, 124). Measurements by Loh & Capelli using UV-OAS resulted in $\beta(CH_3) = 10^{-2}$ in CH_4/H_2 plasmas (125), and recent IRIS studies yielded $\beta(CH)$ near unity in CH_4/Ar plasmas (117) and $\beta(C_3) = 0.1$–0.4 in CH_2F_2/C_3F_8 plasmas, depending on substrate bias and gas ratios (126).

3.5. NH_x Species

N_2 and NH_3 are used for nitride film deposition and polymer surface modification. Tahara et al. used spatially resolved OES to investigate NH_3 and N_2/H_2 plasmas (127)

and found that $T_g \sim 10^3$ K. In N_2/H_2 plasmas, T_g gradually decreases downstream from the plasma arc. For NH_3 plasmas, $\Theta_R(NH)$ drops precipitously. Electrostatic probe measurements suggest that n_e is lower in the NH_3 system; this disparity is likely responsible for changes in $\Theta_R(NH)$. CRDS was applied to NH_x species in Ar/NH_3 plasmas to extract $\Theta_R(NH) = 1920 \pm 100$ K (128). This is comparable to $\Theta_T(NH) = 1750 \pm 100$ K, suggesting energy equilibration of NH. Temperatures and trends found in OES and CRDS studies were comparable and suggest that thermal equilibration of NH_x species occurs readily.

3.5.1. Energetics. Several IRIS studies have focused on NH_x energetics in NH_3 plasmas. Changes in rotational spectra upon interaction with a heated substrate yielded $\Theta_R(NH_2) \sim 340$ K (129), indicating that formation of NH_2 does not involve significant rotational heating. $\Theta_T(NH_2)$ in the molecular beam averaged 500–650 K and was positively correlated with P (19, 21). Θ_T of NH_2 scattered from a substrate, $\Theta_{Tsc}(NH_2)$, was lower than in the beam ($300 \text{ K} < \Theta_{Tsc} < 550$ K), but higher than T_S (300 K). Using an ion-free molecular beam, Θ_{Tsc} was much closer to T_S, indicating that ion-induced processes are responsible for elevated Θ_{Tsc} (19). In addition, Θ_{Tsc} was dependent on substrate material (metals or polymers), with polymeric substrates having a stronger P dependence. This suggests that substrate material influences energy transfer during plasma-surface interactions.

3.5.2. Surface interactions. $\beta(NH)$ and $\beta(NH_2)$ measured in NH_3 plasmas show that the behavior of the two species are affected in very different ways by P, substrate material, and the presence of ions (19, 21, 130). Increases in $S(NH_2)$ with P are accompanied by decreased $S(NH)$, suggesting that NH surface generation comes at the expense of NH_2, potentially via process 2 shown in **Figure 2*a***. As $\Theta_{Tsc}(NH_2) > T_S$, NH_2 surface generation must occur via processes that do not allow full thermal equilibration at the surface (19, 21).

Processing of polymers such as polyethylene (PE) in NH_3/H_2 plasmas is controlled by gas-phase species (131, 132). OES data indicate that N_2, NH, and H are dominant NH_3 decomposition products. Increases in $[H_2]$ in the feed were accompanied by decreases in PE N/C ratios because hydrogen reduces surface NH_x, ultimately promoting formation of volatile NH_x. P dependence data revealed that although low-energy ion bombardment activates the surface for grafting, high-energy bombardment increases sputtering (**Figure 2*a***, *process* 7) and limits grafting efficiency (133). Ishikawa et al. characterized film etching in N_2/H_2 plasmas using in situ ATR-FTIR spectroscopy and electron spin resonance (134). With no substrate bias, treatment resulted in formation of CN and NH moieties in the film. As bias voltage was increased, these disappeared from the spectra, and at bias >200 V, etching was observed. Although surface nitriding may produce etch resistance, N-containing etch products were detected, suggesting that nitrogen both facilitates and inhibits etching. [NH] and $[NH_2]$ CRDS measurements in NH_3/Ar plasmas indicate that Ar^+ undergoes charge transfer reactions with NH_3; subsequent NH_3 decomposition occurs via dissociative recombination. Thus, Ar^+ is largely responsible for the NH_3 breakdown.

4. GLOBAL REMARKS ON PLASMA-SURFACE INTERACTIONS

The studies reviewed above clearly demonstrate that diagnostic tools reveal details of plasma process chemistry. Currently, however, only a limited number of techniques are available to determine β values for plasma species. Given the complexity of plasma-surface interactions, it would be useful to establish some global trends. One characteristic that could be critical is the electronic configuration of unsaturated species (135).

In addition to spectral properties, **Table 2** presents dipole moments and relative surface reactivities (also known as "stickiness" factors) for plasma species. Trends that can be gleaned from these data suggest that several doublet species (SiH, CH, CN) are highly reactive, with $\beta \sim 1$ under all conditions. Other doublets, such as NH_2, OH, and SiF, display moderate β during film deposition (**Table 2**). The observed differences in β of these doublet species could result from relative electronegativities. Molecules with stronger dipole moments (SiF, OH, NH_2) appear to be less reactive than those with smaller dipole moments (CH, SiH, CN). Reactivities may also be related to the availability of surface reaction partners, for example H atoms (28). The sole triplet species listed in **Table 2**, NH, has very low β despite having two unpaired electrons, suggesting that NH may not be an active film precursor. Finally, the isoelectronic singlet species CF_2, SiF_2, and $SiCl_2$ are clearly generated during plasma-surface interactions ($S \gg 1$). This may be related to these species' inherent stability, such that they are extremely probable reaction products. The low β values strongly suggest that MX_2 species (M = Si, C; X = F, Cl) may not be film precursors, although ion-induced production of MX_2 is a significant contributor. Notably, singlet species without strongly electron-withdrawing substituents (SiH_2, C_3) exhibit moderate reactivity, indicating that these species likely contribute to film growth.

Although these statements are generalizations, they represent a beginning for the difficult task of characterizing plasma-surface interactions. Areas requiring continued study include:

1. Measurement of internal and kinetic temperatures for multiple species within a plasma system to determine energy partitioning and kinetics. As evident from the Θ_R and Θ_T measurements discussed above, knowing only one of these does not representatively assess T_g. Moreover, data for only a single plasma species can result in a limited picture of energy partitioning.
2. Continued development of diagnostics applicable to a wider range of plasma species. CRDS is perhaps the closest to meeting this need as it has the widest applicability.
3. Increased focus on measurement of β values during processing to provide broader views of plasma chemistry.

Thus, in situ measurement methods and creation of radical-surface interaction databases to describe contributions of **Figure 2** processes to the overall plasma chemistry are critical. Future efforts will significantly enhance our understanding of process chemistry, with the goal of controlling plasma-surface interactions to create tailored materials.

SUMMARY POINTS

1. Application of multiple diagnostic tools is key to improving and controlling plasma process chemistry.
2. Continued development of diagnostics applicable to a wider range of plasma species is critical to enhancing our understanding of plasma processing.
3. Measurement of internal and kinetic temperatures for multiple species within a plasma system to determine energy partitioning and kinetics will significantly aid numerical modeling efforts.
4. Surface interaction data suggest that molecule-surface interactions are strongly influenced by the molecule's electronic configuration and dipole moment, suggesting possible generalizations for these reactions.

FUTURE ISSUES

1. An increased focus on the measurement of β values during processing to provide broader views of plasma chemistry is needed. Thus, in situ measurement methods and creation of radical-surface interaction databases are critical.
2. Additional progress will be made through development of numerical models utilizing recent experimental data derived from plasma diagnostic tools, which provide more accurate descriptions of the fate of individual species during plasma processing.

DISCLOSURE STATEMENT

The authors are not aware of any biases that might be perceived as affecting the objectivity of this review.

ACKNOWLEDGMENTS

Much of this work was supported by the National Science Foundation. We also acknowledge the assistance of past and current coworkers, Dr. Dongping Liu, Dr. Ina T. Martin, Dr. Patrick R. McCurdy, Ms. Michelle Morgan, Dr. Keri L. Williams, Dr. Jianming Zhang, and Dr. Jie Zhou.

LITERATURE CITED

1. Herman IP. 1996. *Optical Diagnostics for Thin Film Processing*. San Diego: Academic. 783 pp.
2. Selwyn GS. 1993. *Optical Diagnostic Techniques for Plasma Processing*. New York: AVS. 161 pp.

3. Donnelly VM. 1989. Optical diagnostic techniques for low pressure plasmas and plasma processing. In *Plasma Diagnostics*, ed. O Auciello, DF Flamm. Boston: Academic
4. Gottscho RA, Miller TA. 1984. Optical techniques in plasma diagnostics. *Pure Appl. Chem.* 36:189–208
5. Hershkowitz N, Breun RA. 1997. Diagnostics for plasma processing (etching plasmas). *Rev. Sci. Instrum.* 68:880–85
6. Schere JJ, Paul JB, O'Keefe A, Saykally RJ. 1997. Cavity ringdown laser absorption spectroscopy: history, development, and application to pulsed molecular beams. *Chem. Rev.* 97:25–51
7. Freegarde TGM, Hancock G. 1997. A guide to laser-induced fluorescence diagnostics in plasmas. *J. Phys. IV* 7:15–29
8. Donnelly VM, Malyshev MV, Schabel M, Kornblit A, Tai W, et al. 2002. Optical plasma emission spectroscopy of etching plasmas used in Si-based semiconductor processing. *Plasma Sources Sci. Technol.* 11:A26–A30
9. Malyshev MV, Donnelly VM. 1999. Trace rare gases optical emission spectroscopy: nonintrusive method for measuring electron temperatures in low-pressure, low-temperature plasmas. *Phys. Rev. E* 60:6016–29
10. Hancock G, Sucksmith JP, Toogood MJ. 1990. Plasma kinetic measurements using time-resolved actinometry: comparisons with laser-induced fluorescence. *J. Phys. Chem.* 94:3269–72
11. Hebner GA, Miller PA, Woodworth JR. 2000. Overview of Plasma Diagnostic Techniques. In *Handbook of Advanced Plasma Processing Techniques*, ed. RJ Shul, SJ Pearton. Berlin: Springer-Verlag
12. Miller PA, Hebner GA, Jarecki RL. 1998. Optical self-absorption technique for qualitative measurement of excited-state densities in plasma reactors. *J. Vac. Sci. Technol. A* 16:3240–46
13. Amorim J, Baravian G, Jolly J. 2000. Laser-induced resonance fluorescence as a diagnostic technique in nonthermal equilibrium plasmas. *J. Phys. D: Appl. Phys.* 33:R51–65
14. Cunge G, Booth JP, Derouard J. 1996. Absolute concentration measurements by pulsed laser-induced fluorescence in low-pressure gases: allowing for saturation effects. *Chem. Phys. Lett.* 263:645–50
15. Cunge G, Chabert P, Booth JP. 2001. Absolute fluorine atom concentrations in fluorocarbon plasmas determined from NH_3 loss kinetics. *J. Appl. Phys.* 89:7750–55
16. Sakurai T. 2007. Laser-based plasma particle analysis of the surface in a discharge. *Plasma Sources Sci. Technol.* 16:S101–6
17. Amorim J, Baravian G, Sultan G. 1998. Absolute density measurements of ammonia synthesized in N_2-H_2 mixture discharges. *Appl. Phys. Lett.* 68:1915–17
18. Bowles J, McWilliams R, Rynn N. 1994. Direct measurement of velocity space transport in a plasma. *Phys. Plasmas* 1:3814–25
19. Butoi CI, Steen ML, Peers JRD, Fisher ER. 2001. Mechanisms and energy transfer for surface generation of NH_2 during NH_3 plasma processing of metal and polymer substrates. *J. Phys. Chem. B* 105:5957–67

20. Kessels WMM, McCurdy PR, Williams KL, Barker GR, Venturo VA, Fisher ER. 2002. Surface seactivity and plasma energetics of SiH radicals during plasma deposition of silicon-based materials. *J. Phys. Chem. B* 106:2680–89
21. McCurdy PR, Venturo VA, Fisher ER. 1997. Velocity distributions of NH_2 radicals in an NH_3 plasma molecular beam. *Chem. Phys. Lett.* 274:120–26
22. McCurdy PR, Bogart KHA, Dalleska NF, Fisher ER. 1997. A modified molecular beam instrument for the imaging of radicals interacting with surfaces during plasma processing. *Rev. Sci. Instrum.* 68:1684–93
23. Martin IT, Zhou J, Fisher ER. 2006. Correlating ion energies and CF_2 surface production during fluorocarbon plasma processing of silicon. *J. Appl. Phys.* 100:013301
24. Williams KL, Fisher ER. 2003. Mechanisms for deposition and etching in fluorosilane plasma processing. *J. Vac. Sci. Technol. A* 21:1688–701
25. Williams KL, Martin IT, Fisher ER. 2002. On the importance of ions and ion-molecule reactions to plasma-surface interface reactions. *J. Am. Soc. Mass. Spectrom.* 13:518–29
26. Liu D, Martin IT, Fisher ER. 2006. CF_2 surface reactivity during hot filament and plasma-enhanced chemical vapor deposition of fluorocarbon films. *Chem. Phys. Lett.* 430:113–16
27. Zhang J, Williams KL, Fisher ER. 2003. Velocity distributions of SiF and SiF_2 radicals in an SiF_4 plasma molecular beam. *J. Phys. Chem. A* 107:593–97
28. Bogart KHA, Cushing JP, Fisher ER. 1997. Effects of plasma processing parameters on the surface reactivity of $OH(X^2P)$ in tetraethoxysilane/O_2 plasmas during deposition of SiO_2. *J. Phys. Chem. B* 101:10016–23
29. Berden G, Peeters R, Meijer G. 2000. Cavity ring-down spectroscopy: experimental schemes and applications. *Internat. Rev. Phys. Chem.* 19:565–607
30. Booth JP, Cunge G, Biennier L, Romanini D, Kachanov A. 2000. Ultraviolet cavity ring-down spectroscopy of free radicals in etching plasmas. *Chem. Phys. Lett.* 317:631–36
31. Kessels WMM, Hoefnagels JPM, Boogaarts MGH, Schram DC, van de Sanden MCM. 2001. Cavity ring down study of the densities and kinetics of Si and SiH in a remote Ar-H_2-SiH_4 plasma. *J. Appl. Phys.* 89:2065–73
32. Hoefnagels JPM, Barrell Y, Kessels WMM, van de Sanden MCM. 2004. Time-resolved cavity ringdown study of the Si and SiH_3 surface reaction probability during plasma deposition of a-Si:H at different substrate temperatures. *J. Appl. Phys.* 96:4094–106
33. Hoefnagels JPM, Stevens AAE, Boogaarts MGH, Kessels WMM, van de Sanden MCM. 2002. Time-resolved cavity ring-down spectroscopic study of the gas phase and surface loss rates of Si and SiH_3 plasma radicals. *Chem. Phys. Lett.* 360:189–93
34. Yalin AP, Zare RN, Laux CO, Kruger CH. 2002. Temporally resolved cavity ring-down spectroscopy in a pulsed nitrogen plasma. *Appl. Phys. Lett.* 81:1408–10
35. Piejak R, Godyak V, Alexandrovich B. 2001. Validation of current density measurements with a B-dot probe. *Rev. Sci. Instrum.* 72:4002–4

36. Tuszewski M, Tobin JA. 1996. The accuracy of Langmuir probe ion density measurements in low-frequency RF discharges. *Plasma Sources Sci. Technol.* 5:640–47
37. van Hest MFAM, de Graaf A, van de Sanden MCM, Schram DC. 2000. Use of in situ FTIR spectroscopy and mass spectrometry in an expanding hydrocarbon plasma. *Plasma Sources Sci. Technol.* 9:615–24
38. Karecki S, Chatterjee R, Pruette L, Reif R, Vartanian V, et al. 2001. Characterization of iodoheptafluoropropane as a dielectric etchant. III. Effluent analysis. *J. Vac. Sci. Technol. B* 19:1306–18
39. Schmidt M, Foest R, Basner R. 2001. Mass spectrometric diagnostics. *Low Temp. Plasma Phys.* 199:199–227
40. Eddy CR Jr. 2000. Mass spectrometric characterization of plasma etching processes. In *Handbook of Advanced Plasma Processing Techniques*, ed. RJ Shul, SJ Pearton. Berlin: Springer-Verlag
41. Singh H, Coburn JW, Graves DB. 1999. Mass spectrometric detection of reactive neutral species: Beam-to-background ratio. *J. Vac. Sci. Technol. A* 17:2447–55
42. Agarwal S, Quax GWW, van de Sanden MCM, Maroudas D, Aydil ES. 2004. Measurement of absolute radical densities in a plasma using modulated-beam line-of-sight threshold ionization mass spectrometry. *J. Vac. Sci. Technol. A* 22:71–81
43. Benedikt J, Agarwal S, Eijkman D, Vandamme W, Creatore M, van de Sanden MCM. 2005. Threshold ionization mass spectrometry of reactive species in remote Ar/C_2H_2 expanding thermal plasma. *J. Vac. Sci. Technol. A* 23:1400–12
44. Janes J, Banzinger U, Huth C, Hoffmann P, Neumann G, Scheer H-C. 1992. Analysis of large-area beam attacks on surfaces and testing of etching reactions. *Rev. Sci. Instrum.* 63:48–55
45. Ferreira JA, Tabares FL. 2007. Cryotrapping assisted mass spectrometry for the analysis of complex gas mixtures. *J. Vac. Sci. Technol. A* 25:246–51
46. Lopez-Garzon FJ, Domingo-Garcia M, Perez-Mendoza M, Alvarez PM, Gomez-Serrano V. 2003. Textural and chemical surface modifications produced by some oxidation treatments of glassy carbon. *Langmuir* 19:2838–44
47. Motomura H, Imai S, Tachibana K. 2001. Surface reaction processes in C_4F_8 and C_5F_8 plasmas for selective etching of SiO over photo-resist. *Thin Solid Films* 390:134–38
48. Shirafuji T, Motomura H, Tachibana K. 2004. Fourier transform infrared phase-modulated ellipsometry for in situ diagnostics of plasma-surface interactions. *J. Phys. D: Appl. Phys.* 37:R49–R73
49. Schneider L, Peukert W. 2007. Second harmonic generation spectroscopy as a method for in situ and online characterization of particle surface properties. *Part. Part. Sys. Charact.* 23:351–59
50. Simpson GJ. 2001. New tools for surface second-harmonic generation. *Appl. Spectrosc.* 55:16A–32A
51. Kessels WMM, Gielis JJH, Aarts IMP, Leewis CM, van de Sanden MCM. 2004. Spectroscopic second harmonic generation measured on plasma-deposited hydrogenated amorphous silicon thin films. *Appl. Phys. Lett.* 85:4049–51

52. Aarts IMP, Gielis JJH, van de Sanden MCM, Kessels WMM. 2006. Probing hydrogenated amorphous silicon surface states by spectroscopic and real-time second-harmonic generation. *Phys. Rev. B: Condens. Matter* 73:045327
53. Gielis JJH, Gevers PM, Stevens AAE, Beijerinck HCW, van de Sanden MCM, Kessels WMM. 2006. Spectroscopic second-harmonic generation during Ar^+-ion bombardment of Si(100). *Phys. Rev. B: Condens. Matter* 74:1665311
54. Laird RK, Andrews EB, Barrow RF. 1950. Absorption spectrum of CF_2. *Trans. Faraday Soc.* 46:803–5
55. Venkateswarlu P. 1959. On the emission bands of CF_2. *Phys. Rev.* 77:676–80
56. Mathias E, Miller GH. 1965. The decomposition of polytetrafluoroethylene in a glow discharge. *J. Phys. Chem.* 71:2671–75
57. Winters HF, Coburn JW. 1992. Surface science aspects of etching reactions. *Surf. Sci. Rep.* 14:161–269
58. Coburn JW, Winters HF. 1983. Plasma-assisted etching in microfabrication. *Ann. Rev. Mater. Sci.* 13:91–116
59. Coburn JW, Winters HF. 1981. Plasma-etching: a discussion of mechanisms. *CRC Crit. Rev. Solid State Mater. Sci.* 10:119–41
60. Graves DB, Humbird D. 2002. Surface chemistry associated with plasma etching processes. *Appl. Surf. Sci.* 192:72–87
61. Zhang D, Kushner MJ. 2000. Surface kinetics and plasma equipment model for Si etching by fluorocarbon plasmas. *J. Appl. Phys.* 87:1060–69
62. Martin IT, Dressen B, Boggs M, Liu Y, Henry CS, Fisher ER. 2007. Plasma modification of PDMS microfluidic devices for control of electroosmotic flow. *Plasma Process. Polym.* 4:414–24
63. Kiss LDB, Nicolai J-P, Conner WT, Sawin HH. 1992. CF and CF_2 actinometry in a CF_4/Ar plasma. *J. Appl. Phys.* 71:3186–92
64. Booth JP, Cunge G, Neuilly F, Sadeghi N. 1998. Absolute radical densities in etching plasmas determined by broad-band UV absorption spectroscopy. *Plasma Sources Sci. Technol.* 7:423–30
65. Booth JP, Abada H, Chabert P, Graves DB. 2005. CF and CF_2 radical kinetics and transport in a pulsed CF_4 ICP. *Plasma Sources Sci. Technol.* 14:273–82
66. Booth JP, Cunge G, Chabert P, Sadeghi N. 1999. CF_x radical production and loss in a CF_4 reactive ion etching plasma: fluorine rich conditions. *J. Appl. Phys.* 85:3097–107
67. Singh H, Coburn JW, Graves DB. 2001. Measurements of neutral and ion composition, neutral temperature, and electron energy distribution function in a CF_4 inductively coupled plasma. *J. Vac. Sci. Technol. A* 19:718–29
68. Miyoshi Y, Miyauchi M, Oguni A, Makabe T. 2006. Optical diagnostics for plasma-surface interaction in CF_4/Ar radio-frequency inductively coupled plasma during Si and SiO_2 etching. *J. Vac. Sci. Technol. A* 24:1718–24
69. Schabel MJ, Donnelly VM, Kornblit A, Tai WW. 2002. Determination of electron temperature, atomic fluorine concentration, and gas temperature in inductively coupled fluorocarbon/rare gas plasmas using optical emission spectroscopy. *J. Vac. Sci. Technol. A* 20:555–63

70. Nagai M, Hori M. 2007. Temperature and density of CF radicals in 60 MHz capacitively coupled fluorocarbon gas plasma. *Jpn. J. Appl. Phys., Part 1* 46:1176–80
71. Steffens KL, Sobolewski MA. 2004. A technique for temperature mapping in fluorocarbon plasmas using planar laser-induced fluorescence of CF. *J. Appl. Phys.* 96:71–81
72. Hebner GA, Miller PA. 2000. Electron and negative ion densities in C_2F_6 and CHF_3 containing inductively coupled discharges. *J. Appl. Phys.* 87:7660–66
73. Sasaki K, Kawai Y, Suzuki C, Kadota K. 1997. Kinetics of fluorine atoms in high-density carbon tetrafluoride plasmas. *J. Appl. Phys.* 82:5938–43
74. Sugai H, Nakamura K, Hikosaka Y, Nakamura M. 1995. Diagnostics and control of radicals in an inductively coupled etching reactor. *J. Vac. Sci. Technol. A* 13:887–93
75. Zhou B, Joseph EA, Sant SP, Liu Y, Radhakrishnan A, et al. 2005. Effect of surface temperature on plasma-surface interactions in an inductively coupled modified gaseous electronics conference reactor. *J. Vac. Sci. Technol. A* 23:1657–67
76. Butoi CI, Mackie NM, Williams KL, Capps NE, Fisher ER. 2000. Ion and substrate effects on surface reactions of CF_2 using C_2F_6, C_2F_6/H_2, and hexafluoropropylene oxide plasmas. *J. Vac. Sci. Technol. A* 18:2685–98
77. Mackie NM, Venturo VA, Fisher ER. 1997. Surface reactivity of CF_2 radicals measured using laser-induced fluorescence and C_2F_6 plasma molecular beams. *J. Phys. Chem. B* 101:9425–28
78. Senesi GS, Aloia ED, Gristina R, Favia P, d'Agostino R. 2007. Surface characterization of plasma deposited nano-structured fluorocarbon coatings for promoting in vitro cell growth. *Surf. Sci.* 601:1019–25
79. Hori M, Goto T. 2007. Insights into sticking of radicals on surface for smart plasma nano-processing. *Appl. Surf. Sci.* 253:6657–71
80. Cunge G, Booth JP. 1999. CF_2 production and loss mechanisms in fluorocarbon discharges: fluorine-poor conditions and polymerization. *J. Appl. Phys.* 85:3952–59
81. Singh H, Coburn JW, Graves DB. 2000. Surface loss coefficients of CF_x and F radicals on stainless steel. *J. Vac. Sci. Technol. A* 18:2680–84
82. Hikosaka Y, Toyoda H, Sugai H. 1993. Drastic change in CF_2 and CF_3 kinetics induced by hydrogen addition into a CF_4 etching plasma. *Jpn. J. Appl. Phys., Part 1* 32:L690–93
83. Capps NE, Mackie NM, Fisher ER. 1998. Surface interactions of CF_2 radicals during deposition of amorphous fluorocarbon films from CHF_3 plasmas. *J. Appl. Phys.* 84:4736–43
84. Martin IT, Fisher ER. 2004. Ion effects on CF_2 surface interactions during C_3F_8 and C_4F_8 plasma processing of Si. *J. Vac. Sci. Technol. A* 22:2168–76
85. Cruden BA, Gleason KK, Sawin HH. 2001. Time resolved UV absorption spectroscopy of pulsed fluorocarbon plasmas. *J. Appl. Phys.* 89:915–22
86. Fisher ER. 2004. A review of plasma-surface interactions during processing of polymeric materials measured using the IRIS technique. *Plasma Process. Polym.* 1:13–27

87. Butterbaugh JW, Grey DC, Sawin HH. 1991. Plasma-surface interactions in fluorocarbon etching of silicon dioxide. *J. Vac. Sci. Technol. B* 9:1461–70
88. Gray DC, Sawin HH, Butterbaugh JW. 1991. Quantification of surface film formation effects in fluorocarbon plasma etching of polysilicon. *J. Vac. Sci. Technol. A* 9:779–85
89. Fuoco ER, Hanley L. 2002. Large fluorocarbon ions can contribute to film growth during plasma etching of silicon. *J. Appl. Phys.* 92:37–44
90. Wijesundara MBJ, Zajac G, Fuoco ER, Hanley L. 2001. Aging of fluorocarbon thin films deposited on polystyrene from hyperthermal $C_3F_5^+$ and CF_3^+ ion beams. *J. Adhes. Sci. Technol.* 15:599–612
91. Goyette AN, Wang Y, Misakian M, Olthoff JK. 2000. Ion fluxes and energies in inductively coupled radio-frequency discharges containing C_2F_6 and c-C_4F_8. *J. Vac. Sci. Technol. A* 18:2785–90
92. Lee HU, Deneufville JP, Ovshinsky SR. 1983. Laser-induced fluorescence detection of reactive intermediates in diffusion flames and in glow-discharge deposition reactors. *J. Non-Crystal. Solids* 59–6:671–74
93. Mutsukura N, Ohuchi M, Satoh S, Machi Y. 1983. The analysis of an SiF_4 plasma in an R.F. glow discharge for preparing fluorinated amorphous silicon thin films. *Thin Solid Films* 109:47–57
94. Martin RW, Merer AJ. 1973. Electronic transition of SiF. *Can. J. Phys.* 51:634–43
95. Johns JWC, Barrow RF. 1958. The band spectrum of silicon monofluoride, SiF. *Proc. Phys. Soc. Lond.* 71:476–84
96. Lee S, Tien Y-C, Hsu C-F. 1999. Direct spectroscopic evidence of the influence of chamber wall condition on oxide etch rate. *Plasma Chem. Plasma Process.* 19:285–98
97. Hebner GA. 2002. Spatially resolved CF, CF_2, SiF and SiF_2 densities in fluorocarbon containing inductively driven discharges. *Appl. Surf. Sci.* 192:161–75
98. Cunge G, Chabert P, Booth JP. 1997. Laser-induced fluorescence detection of SiF_2 as a primary product of Si and SiO_2 reactive ion etching with CF_4 gas. *Plasma Sources Sci. Technol.* 6:349–60
99. Giapis KP, Minton TK. 1996. Monitoring of direct reactions during etching of silicon. *Mater. Res. Soc. Symp. Proc.* 406:33–38
100. Giapis KP, Moore TA, Minton TK. 1995. Hyperthermal neutral beam etching. *J. Vac. Sci. Technol. A* 13:959–65
101. Williams KL, Fisher ER. 2003. Substrate temperature effects on surface reactivity of SiF_x ($x = 1, 2$) radicals in fluorosilane plasmas. *J. Vac. Sci. Technol. A* 21:1024–32
102. Matsuda A. 2004. Thin-film silicon growth process and solar cell application. *Jpn. J. Appl. Phys., Part 1* 43:7909–20
103. Sriraman S, Aydil ES, Maroudas D. 2004. Growth and characterization of hydrogenated amorphous silicon thin films from SiH_2 radical precursor: atomic-scale analysis. *J. Appl. Phys.* 95:1792–804

104. Kessels WMM, Hoefnagels JPM, van den Oever PJ, Barrell Y, van de Sanden MCM. 2003. Temperature dependence of the surface reactivity of SiH_3 radicals and the surface silicon hydride composition during amorphous silicon growth. *Surf. Sci.* 547:L865–70
105. Kessels WMM, Marra DC, van de Sanden MCM, Aydil ES. 2002. In situ probing of surface hydrides on hydrogenated amorphous silicon using attenuated total reflection infrared spectroscopy. *J. Vac. Sci. Technol. A* 20:781–89
106. Stamou S, Mataras D, Rapakoulias D. 1998. Spatial rotational temperature and emission intensity profiles in silane plasmas. *J. Phys. D: Appl. Phys.* 31:2513–20
107. Zhou J, Zhang J, Fisher ER. 2005. Effects of argon dilution on the translational and rotational temperatures of SiH in silane and disilane plasmas. *J. Phys. Chem. A* 109:10521–26
108. Kessels WMM, van de Sanden MCM, Severens RJ, Schram DC. 2000. Surface reaction probability during fast deposition of hydrogenated amorphous silicon with a remote silane plasma. *J. Appl. Phys.* 87:3313–20
109. Hertl M, Jolly J. 2000. Laser-induced fluorescence detection and kinetics of SiH_2 radicals in $Ar/H_2/SiH_4$ RF discharges. *J. Phys. D: Appl. Phys.* 33:381–88
110. Perrin J, Shiratani M, Kae-Nune P, Videlot H, Jolly J, Guillon J. 1998. Surface reaction probabilities and kinetics of H, SiH_3, Si_2H_5, CH_3, and C_2H_5 during deposition of a-Si:H and a-C:H from H_2, SiH_4, and CH_2 discharges. *J. Vac. Sci. Technol. A* 16:278–89
111. Bakos T, Valipa MS, Maroudas D. 2007. Interactions between radical growth precursors on plasma-deposited silicon thin-film surfaces. *J. Chem. Phys.* 126:114704
112. Singh T, Valipa MS, Mountziaris TJ, Maroudas D. 2007. First-principles theoretical analysis of sequential hydride dissociation on surfaces of silicon thin films. *Appl. Phys. Lett.* 90:251915
113. Sriraman S, Ramalingam S, Aydil ES, Maroudas D. 2000. Abstraction of hydrogen by Si radicals from hydrogenated amorphous silicon wafers. *Surf. Sci.* 459:L475–81
114. Zhou J, Martin IT, Adams E, Liu D, Fisher ER. 2006. Investigation of inductively coupled Ar and CH_4/Ar plasmas and the effect of ion energy on DLC film properties. *Plasma Sources Sci. Technol.* 15:714–26
115. von Keudell A, Kim I, Consoli A, Schulze M, Yangua-Gil A, Bendikt J. 2007. The search for growth precursors in reactive plasmas: from nanoparticles to microplasmas. *Plasma Sources Sci. Technol.* 16:S94–100
116. Liu D, Zhou J, Fisher ER. 2007. Correlation of gas-phase composition with film properties in the plasma-enhanced chemical vapor deposition of hydrogenated amorphous carbon nitride films. *J. Appl. Phys.* 101:023304
117. Zhou J, Fisher ER. 2006. Surface reactivity and energetics of CH radicals during plasma deposition of hydrogenated diamond-like carbon films. *J. Phys. Chem. B* 110:21911–19
118. van Hest MFAM, Haartsen JR, van Weert MHM, Schram DC, van de Sanden MCM. 2003. Analysis of the expanding thermal argon–oxygen plasma gas phase. *Plasma Sources Sci. Technol.* 12:539–53

119. Benedikt J, Schram DC, van de Sanden MCM. 2005. Detailed TIMS study of Ar/C_2H_2 expanding thermal plasma: identification of a-C:H film growth precursors. *J. Phys. Chem. A* 109:10153–67
120. Benedikt J, Woen RV, van Mensfoort SLM, Perina V, Hong J, van de Sanden MCM. 2003. Plasma chemistry during the deposition of a-C:H films and its influence on film properties. *Diamond Rel. Mater.* 12:90–97
121. von Keudell A, Schwarz-Selinger T, Jacob W. 2001. Simultaneous interaction of methyl radicals and atomic hydrogen with amorphous hydrogenated carbon films. *J. Appl. Phys.* 89:2979–86
122. von Keudell A, Meier M, Schwarz-Selinger T. 2001. Simultaneous interaction of methyl radicals and atomic hydrogen with amorphous hydrogenated carbon films, as investigated with optical in situ diagnostics. *Appl. Phys. A* 72:551–56
123. Sugai H, Toyoda H. 1992. Appearance mass spectrometry of neutral radicals in radio frequency plasmas. *J. Vac. Sci. Technol. A* 10:1193–200
124. Kojima H, Toyoda H, Sugai H. 1989. Observation of CH_2 radical and comparison with CH_3 radical in an rf methane discharge. *Appl. Phys. Lett.* 55:1292–94
125. Loh MH, Capelli MA. 1997. CH_3 detection in a low-density supersonic arcjet plasma during diamond synthesis. *Appl. Phys. Lett.* 70:1052–54
126. Liu D, Fisher ER. 2007. Surface reactivities of C_3 radicals during the deposition of fluorocarbon and hydrocarbon films. *J. Vac. Sci. Technol. A* 25:1519–23
127. Tahara H, Ando Y, Onoe K, Yoshikawa T. 2002. Plasma plume characteristics of supersonic ammonia and nitrogen/hydrogen-mixture DC plasma jets for nitriding under low-pressure environment. *Vacuum* 65:311–18
128. van den Oever PJ, van Helden JH, Lamers CCH, Engeln R, Schram DC, et al. 2005. Density and production of NH and NH_2 in an Ar-NH_3 expanding plasma jet. *J. Appl. Phys.* 98:093301
129. McCurdy PR, Butoi CI, Williams KL, Fisher ER. 1999. Surface interactions of NH_2 radicals in NH_3 plasmas. *J. Phys. Chem. B* 103:6919–29
130. Steen ML, Kull KR, Fisher ER. 2002. Comparison of surface interactions for NH and NH_2 radicals on polymer and metal substrates during NH_3 plasma processing. *J. Appl. Phys.* 92:55–63
131. Cicala G, Bruno G, Capezzuto P, Favia P. 1996. Photoelectron spectroscopy study of amorphous silicon-carbon alloys deposited by plasma-enhanced chemical vapor deposition. *J. Mater. Res.* 11:3017–23
132. Creatore M, Cicala G, Favia P, Lamendola R, d'Agostino R. 1999. Selective grafting of amine groups on polyethylene by means of modulated RF NH_3 plasmas. *Mater. Res. Soc. Symp. Proc.* 544:115–20
133. Cicala G, Creatore M, Favia P, Lamendola R, d'Agostino R. 1999. Modulated rf discharges as an effective tool for selecting exciting species. *Appl. Phys. Lett.* 75:37–39
134. Ishikawa K, Yamaoka Y, Nakamura M, Yamazaki Y, Yamasaki S, et al. 2006. Surface reactions during etching of organic low-*k* films by plasmas of N_2 and H_2. *J. Appl. Phys.* 99:083305

135. Liu D, Martin IT, Zhou J, Fisher ER. 2006. Radical surface interactions during film deposition: a sticky situation? *Pure Appl. Chem.* 78:1187–202
136. Iordanova S, Koleva I. 2007. Optical emission spectroscopy diagnostics of inductively-driven plasmas in argon gas at low pressures. *Spectrochim. Acta B* 62:344–56
137. Hueso JL, Gonzalez-Flipe AR, Cotrino J, Caballero A. 2005. Plasma chemistry of NO in complex gas mixtures excited with a surfatron launcher. *J. Phys. Chem. A* 109:4930–38
138. Balfour WJ, Cao JY, Prasad CVV, Qian CXW. 1994. Laser-induced fluorescence spectroscopy of the a^1P_u-$X^1S^+_g$ transition in jet-cooled C_3. *J. Chem. Phys.* 101:10343–49
139. Luque J, Juchmann W, Jeffries JB. 1997. Spatial density distributions of C_2, C_3, and CH radicals by laser-induced fluorescence in a diamond depositing dc-arcjet. *J. Appl. Phys.* 82:2072–81
140. Ito H, Ichimura SY, Namiki KC, Saitoh H. 2003. Absolute density and sticking probability of the CN(X^2S^+) radicals produced by the dissociative excitation reaction of BrCN with the microwave discharge flow of Ar. *Jpn. J. Appl. Phys., Part 1* 42:7116–21
141. Ushirozawa Y, Matsuda H, Wagatsuma K. 2004. Determination of fluorine in copper by radio-frequency-powered glow-discharge plasma source emission spectroscopy associated with laser ablation sampling. *Jpn. Soc. Anal. Chem.* 53:699–703
142. Foest R, Olthoff JK, VanBrunt RJ, Benck EC, Roberts JR. 1996. Optical and mass spectrometric investigations of ions and neutral species in SF_6 radio-frequency discharges. *Phys. Rev. E* 54:1876–87
143. Suzuki C, Sasaki K, Kadota K. 1999. Formation of C_2 radicals in high-denisty C_4F_8 plasmas studied by laser-induced fluorescence. *Jpn. J. Appl. Phys., Part 1* 38:6896–901
144. Liu D, Martin IT, Fisher ER. 2008. *J. Appl. Phys.* Comparison of CH, C_3, CHF, and CF_2 surface reactivities during plasma enhanced chemical vapor deposition of fluorocarbon films. Work. Pap., Dep. Chem., Colo. State Univ.
145. Gottscho RA, Burton RH, Davis GP. 1982. Radiative lifetime and collisional quenching of carbon monochloride (A^2D) in an alternating current glow discharge. *J. Chem. Phys.* 77:5298–301
146. Skromme BJ, Liu W, Jensen KF, Giapis KP. 1994. Effects of C incorporation on the luminescence properties of the ZnSe grown by metalorganic chemical vapor deposition. *J. Cryst. Growth* 138:338–45
147. Hu X, Zhao G-B, Janardhan Garikipati SVB, Nicholas K, Legowski SF, Radosz S. 2005. Laser-induced fluorescence (LIF) probe for in-situ nitric oxide concentration measurement in a nonthermal pulsed corona discharge plasma reactor. *Plasma Chem. Plasma Process.* 25:351–70
148. Fresnet F, Baravian G, Pasquiers S, Postel C, Puech V, et al. 2000. Time-resolved laser-induced fluorescence study of NO removal plasma technology in N_2/NO mixtures. *J. Phys. D: Appl. Phys.* 33:1315–22

149. Fisher ER, Ho P, Breiland WG, Buss RJ. 1993. Temperature dependence of the reactivity of OH(X^2II) with oxidized silicon nitride and PMMA film surfaces. *J. Phys. Chem.* 97:10287–94
150. Donnelly VM, Herman IP, Cheng CC, Guinn KV, Donnelly VM, et al. 1996. Surface chemistry during plasma etching of silicon. *Pure Appl. Chem.* 68:1071–74
151. Greenberg KE, Hargis PJ Jr. 1990. Laser-induced-fluorescence detection of sulfur monoxide and sulfur dioxide in sulfur hexafluoride/oxygen plasma-etching discharges. *J. Appl. Phys.* 68:505–11